Optimal illumination for three-image photometric stereo acquisition of texture

Andy Spence and Mike Chantler[1]

Abstract - **The optimal placement of the illumination for three-image photometric stereo acquisition of smooth and rough surface textures is derived and verified experimentally. The sensitivities of the scaled surface normal elements are derived and used to provide expressions for the noise variances. An overall figure of merit is developed by considering image-based rendering (i.e. relighting) of Lambertian surfaces. This metric is optimised with respect to the illumination angles. The optimal separation between the tilt angles of successive illumination vectors was found to be 120°. The optimal slant angle was found to be 90° for smooth surface textures and 55° for rough surface textures.**

I. INTRODUCTION

Photometric stereo (PS) is an important technique for the acquisition, analysis and visualisation of surface texture. It uses three or more images captured from a single viewpoint of a surface illuminated from different directions to estimate relief and reflectance information. Woodham demonstrated that three images are sufficient for non-shadowed Lambertian surfaces [1]. Later papers refined and modified the technique to cope with shadows, specularities and interreflections [9,11,12,13,14,15]. However, the basic three-image algorithm is economical and often proves good results. It is also employed in more robust approaches, e.g. 5 image photometric stereo in which the darkest and lightest pixels are discarded [9].

For maximum accuracy in PS it is commonly acknowledged that the slant angle should be maximised whilst minimising shadows [1]. Furthermore, the illumination vectors should not be co-planar [1].

Whilst these guidelines are useful, the choice of illumination vectors is still very much down to the experimenter's discretion. The fact that side lighting acts as a directional filter of the surface height function [16] suggests that the signal-to-noise ratio could be maximised by distributing the illumination tilt angles equally through 360°. However, this has never been formally investigated.

This paper therefore develops a formal expression for the overall signal-to-noise ratio for three image PS. This is optimised over illumination tilt and slant angles to derive the optimal set of lighting conditions. These are verified using a set of real surface textures.

The paper is organised as follows. First we briefly review three image PS and derive expressions for the signal-to-noise ratios for the *scaled surface normals.* We use these to provide an overall figure of merit which is optimised over the illumination angles. These results are compared with empirically derived figures.

II. THREE-IMAGE PHOTOMETRIC STEREO

Assuming fronto-planar imaging of Lambertian surface textures, the irradiance due to a surface element at the point (x,y) may be expressed as:

$$i(x,y) = \rho(x,y)\mathbf{l}.\mathbf{n}(x,y) \tag{1}$$

where: $\rho(x,y)$ is the albedo, $\mathbf{n}(x,y)$ is the surface normal and $\mathbf{l}$ is the illumination vector.

We define $\mathbf{l}$ in terms of slant angle, σ (the angle $\mathbf{l}$ makes with the z-axis) and the tilt angle, τ (the angle $\mathbf{l}$ makes with the x-axis when projected onto the x-y plane). These parameters measure latitude and longitude respectively. Thus:

$$\mathbf{l} = (l_x, l_y, l_z) = (\cos\tau \sin\sigma, \sin\tau \sin\sigma, \cos\sigma) \tag{2}$$

Substituting the *scaled surface normal*

$$\mathbf{t}(x,y) = (t_x, t_y, t_z)^T = \rho(x,y)\mathbf{n}(x,y) \tag{3}$$

into (1) gives:

$$i(x,y) = \mathbf{l}.\mathbf{t}(x,y) \tag{4}$$

Using three images taken under three different illumination vectors provides:

$$\mathbf{i}(x,y) = \begin{bmatrix} i_1(x,y) \\ i_2(x,y) \\ i_3(x,y) \end{bmatrix} = \begin{bmatrix} \mathbf{l}_1 \\ \mathbf{l}_2 \\ \mathbf{l}_3 \end{bmatrix} \mathbf{t}(x,y) \tag{5}$$

solving for $\mathbf{t}(x,y)$ gives

$$\mathbf{t}(x,y) = \mathbf{L}^{-1}\mathbf{i}(x,y) \tag{6}$$

where $\mathbf{L}$ is the illumination matrix $(\mathbf{l}_1, \mathbf{l}_2, \mathbf{l}_3)^T$.

Equation (6) is the basic photometric stereo equation which can be used with SVD to estimate the set of scaled surface normals. These data may be used directly for relighting or for the calculation of albedo $\rho(x, y)$ and unit normals $\mathbf{n}(x, y)$.

III. DERIVATION OF NOISE EXPRESSIONS

We now derive expressions for the noise in the estimates of the scaled surface normals. These are formulated in terms of the input image noise and the illumination angles. It is these functions which are minimised in order to determine the optimal lighting conditions.

As equation (6) is linear the noise in $\mathbf{t}$ can be derived from the sensitivities of each surface normal element t_x, t_y, & t_z to changes in the input image intensities i_1, i_2, & i_3.

[1] Andy Spence and Mike Chantler are with the Texture Lab, Heriot-Watt University, Edinburgh, Scotland (M.J.Chantler@hw.ac.uk)

These nine sensitivities ($\partial t_x/\partial i_1$ etc.) are combined to provide a single figure of merit which is optimised with respect to the illumination angles [17].

For the sake of brevity we present a derivation that assumes the three illumination vectors have the same slant angle. This produces the same results as using independent slant angles while allowing the equations to be of a manageable size for presentation.

A Sensitivity

With constant slant angle σ and tilt angles τ_i where $i=1,2,3$, the illumination matrix **L** is:

$$\mathbf{L}=\begin{bmatrix}\cos\tau_1\sin\sigma & \sin\tau_1\sin\sigma & \cos\sigma\\ \cos\tau_2\sin\sigma & \sin\tau_2\sin\sigma & \cos\sigma\\ \cos\tau_3\sin\sigma & \sin\tau_3\sin\sigma & \cos\sigma\end{bmatrix} \tag{7}$$

Substituting the inverse of this into equation (6) provides expressions for each component of the scaled surface normals:

$$t_x=-\left(\frac{(\sin\tau_3-\sin\tau_2)i_1+(\sin\tau_1-\sin\tau_3)i_2+(\sin\tau_2-\sin\tau_1)i_3}{K\sin\sigma}\right) \tag{8}$$

$$t_y=-\left(\frac{(\cos\tau_2-\cos\tau_3)i_1+(\cos\tau_3-\cos\tau_1)i_2+(\cos\tau_1-\cos\tau_2)i_3}{K\sin\sigma}\right) \tag{9}$$

$$t_z=\left(\frac{\sin(\tau_3-\tau_2)i_1+\sin(\tau_1-\tau_3)i_2+\sin(\tau_2-\tau_1)i_3}{K\cos\sigma}\right) \tag{10}$$

where: $K=\sin(\tau_3-\tau_2)+\sin(\tau_1-\tau_3)+\sin(\tau_2-\tau_1)$

Differentiating equations (8-10) with respect to each of the three image intensities provides nine sensitivity expressions. Three are given below - one example for each element of **t**.

$$\frac{\partial t_x}{\partial i_1}=-\left(\frac{\sin\tau_3-\sin\tau_2}{K\sin\sigma}\right) \tag{11}$$

$$\frac{\partial t_y}{\partial i_1}=-\left(\frac{\cos\tau_2-\cos\tau_3}{K\sin\sigma}\right) \tag{12}$$

$$\frac{\partial t_z}{\partial i_1}=\left(\frac{\sin(\tau_3-\tau_2)}{K\cos\sigma}\right) \tag{13}$$

The sensitivities with respect to changes in i_2 and i_3 are similar and will be referred to as equations (14-19) [17].

B Noise in the Scaled Surface Normal Estimates

If we assume that the noise in each of the three input images is Gaussian, independent and of variance $\bar{\sigma}_i$ then the variance of the noise in t_x is given by :

$$\sigma_{t_x}=\bar{\sigma}_i\sqrt{\left(\frac{\partial t_x}{\partial i_1}\right)^2+\left(\frac{\partial t_y}{\partial i_2}\right)^2+\left(\frac{\partial t_z}{\partial i_3}\right)^2} \tag{20}$$

In order to aid comparison with the empirical results we use the noise ratio:

$$\frac{\sigma_{t_x}}{\bar{\sigma}_i}=\sqrt{\left(\frac{\partial t_x}{\partial i_1}\right)^2+\left(\frac{\partial t_y}{\partial i_2}\right)^2+\left(\frac{\partial t_z}{\partial i_3}\right)^2} \tag{21}$$

Substituting equations (11-13) into (21) gives the full equation for the noise ratio for t_x. Noise ratio expressions for the *y* and *z* components are similarly obtained.

Thus given the variance of the noise in the three input images we may estimate the noise in each of the three scaled surface normal component fields (t_x, t_y, t_z).

C A Single Figure of Merit

It is obviously in our interest to minimise each of the three noise ratios. However, for optimisation purposes we require a single objective function. These functions should be formulated taking into account the intended use of the output data. We have chosen to consider image-based rendering applications. The intensity of a 'relit' pixel under arbitrary illumination can be expressed as follows :

$$\begin{aligned} i_{relight}(x,y) &= t_x(x,y)\cos\tau\sin\sigma \\ &\quad + t_y(x,y)\sin\tau\sin\sigma + t_z(x,y)\cos\sigma \end{aligned} \tag{22}$$

This is simply a weighted sum of the elements of **t**. Therefore we choose our figure of merit to be the variance of the sum of the t_x, t_y, and t_z noise processes. We assume that these noise processes are highly correlated and hence our figure of merit is given by :

$$\begin{aligned} M_{rough} &= \sqrt{\left(\frac{\partial t_x}{\partial i_1}\right)^2+\left(\frac{\partial t_x}{\partial i_2}\right)^2+\left(\frac{\partial t_x}{\partial i_3}\right)^2} \\ &\quad + \sqrt{\left(\frac{\partial t_y}{\partial i_1}\right)^2+\left(\frac{\partial t_y}{\partial i_2}\right)^2+\left(\frac{\partial t_y}{\partial i_3}\right)^2} \\ &\quad + \sqrt{\left(\frac{\partial t_z}{\partial i_1}\right)^2+\left(\frac{\partial t_z}{\partial i_2}\right)^2+\left(\frac{\partial t_z}{\partial i_3}\right)^2} \end{aligned} \tag{23}$$

Substituting (11-19) into (23) provides the final expression which is optimised over the illumination angles. This is straightforward to develop but lengthy and is therefore not reproduced here.

D Smooth Surfaces

For smoother surfaces we may make an additional simplification. If the surface slopes are low (e.g. less than 15°) then following Kube & Pentland [10] we can use a Taylor's series expansion of Lambert's law and ignore the higher order terms. In this case t_z tends to a constant (the local albedo) and can be ignored for the purposes of a sensitivity analysis. The figure of merit for a smooth surface is therefore:

$$M_{smooth}=\sqrt{\left(\frac{\partial t_x}{\partial i_1}\right)^2+\left(\frac{\partial t_x}{\partial i_2}\right)^2+\left(\frac{\partial t_x}{\partial i_3}\right)^2}+\sqrt{\left(\frac{\partial t_y}{\partial i_1}\right)^2+\left(\frac{\partial t_y}{\partial i_2}\right)^2+\left(\frac{\partial t_y}{\partial i_3}\right)^2} \tag{24}$$

In this case equations (11, 12, 14, 15, 17 & 18) are substituted into (24) and optimised over the illumination angles.

IV. Empirical Determination of Noise

The temporal noise in the input to and the output from the photometric stereo algorithm (6) was estimated over a range of illumination conditions.

For each illumination condition [σ, τ_1, τ_2, τ_3] three sets of ten input images $i_1(x,y)$, $i_2(x,y)$ and $i_3(x,y)$ of a real isotropic texture were collected.

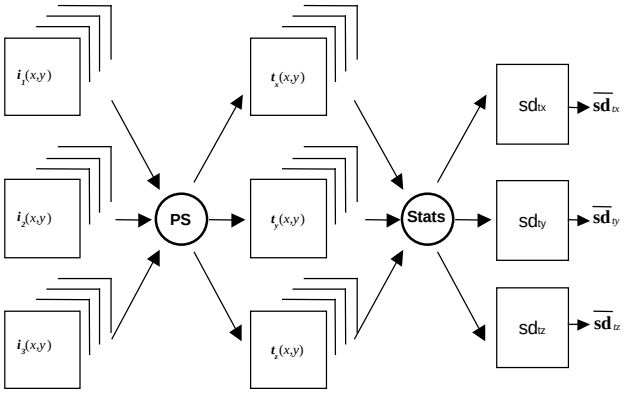

Fig. 1. Empirical estimation of mean temporal input and output noise

This allowed the basic PS equation (6) to be applied ten times for each illumination condition; three sets of ten output images $t_x(x,y)$, $t_y(x,y)$ and $t_z(x,y)$ were hence generated. This provided 60 images which were used to estimate the per-pixel standard variation $sd(x,y)$ of the input and output images. The averages of the resulting 6 standard variation images were calculated to provide estimates of the 6 temporal pixel noise processes in $i_1(x,y)$, $i_2(x,y)$, $i_3(x,y)$, $t_x(x,y)$, $t_y(x,y)$ and $t_z(x,y)$. These figures were used to provide estimates of the input and output noise ratios by combining them in a similar manner to equations (23) and (24).

V. Experiments

Two main types of experiment were conducted: either the tilt angle (τ_3) of the third input image was varied, or alternatively the slant angle of all three images (σ) was varied.

A *Tertiary tilt angle sweep (variation of τ_3)*

In these experiments the primary and secondary tilt angles τ_1 & τ_2 together with the slant angle σ were held constant whilst the tertiary tilt angle τ_3 was swept through a complete rotation in 10° intervals (Figure 2). Images were captured at 10° intervals over a complete rotation for one slant angle to generate 360 images.

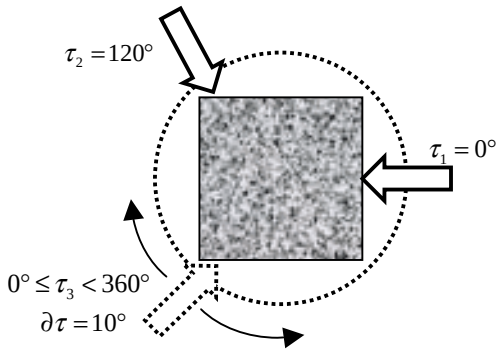

Fig. 2. Example of range of illumination conditions for the tilt angle experiments.

B *Slant angle ramp (variation of σ)*

In a second study the effect of changing the slant angle was investigated. Images were captured for five different tilt angle positions, corresponding to illumination conditions of particular interest. Under each of these conditions the slant angle was varied between 35° to 70° in increments of 5°.

VI. Results

Theoretical estimates of the figures of merit M_{rough} and M_{smooth} were compared against empirically derived measurements for both the *tertiary tilt angle* and *slant angle ramp* experiments.

In addition the theoretical expressions were optimised to determine the 'best' illumination conditions. That is, expansions of equations (23) & (24) were optimised using Nelder & Mead.

Results are presented for both rough and smooth surface metrics.

A *Tertiary tilt angle sweep (variation of τ_3)*

These results are shown in Figures 3 & 4. The noticeable feature common to both graphs is that the noise ratio goes off the scale as the tertiary tilt angle approaches values corresponding to the primary and secondary angles. This is the planar situation when the inverse of the illumination matrix does not exist. In this case it is therefore not possible to solve the system of equations for the unknowns.

The most interesting feature common to both graphs is that there exists a tertiary tilt angle which corresponds to a minimum. This is approximately 240° for the [0°,120°,x°] illumination condition set as highlighted on the plot. However, in the [0°,90°,x°] case the optimal tertiary tilt angle is not 180° but around 225°. This means that McGunnigle's PS scheme [5] although straightforward to solve is not quite optimal.

It is noted that the graphs presented in this section correspond to rough surface textures. Those for smooth surfaces exhibit similar behaviour [17].

B *Slant angle ramp (variation of σ)*

In this case it is actually the difference in behaviour between the two kinds of surfaces which is interesting. Relevant plots are presented for rough and smooth surfaces for the [0°,120°,240°] illumination condition set whilst those for [0°,90°,180°] can be found in [17].

Figure 5 demonstrates that with regard to minimising our figure of merit for a texture of rough surface, a slant angle of about 55° is optimal. However, different behaviour is observed for a smooth surface (Figure 6). The minimum no longer corresponds to 55° but has increased beyond the range of the graph. Extrapolation appears to suggest that in this case a slant angle of 90° is optimal. This observation will later be confirmed by minimisation (See section C).

C *Minimisation*

In this case the value of a constant slant angle corresponding to a minimum was to be determined in

addition to the tilt angles. The minimum was again found to occur for tilt angles of 0°,120° & 240° for both rough and smooth surfaces. With regard to the slant angle, however, it was established that the value corresponding to the minimum depends on the nature of the surface. For a smooth surface it was found to be 90° whereas for a rough surface it was approximately 55°.

This finding can be understood by considering the derived expressions for the sensitivities and figures of merit. In equations (11-13) it is noted that the sensitivity of both t_x & t_y is inversely proportional to $\sin\sigma$ whilst for t_z the equivalent term is $\cos\sigma$. For the smooth surface model where the figure of merit only considers the effect of the primary and secondary elements of **t**, this means that the slant angle should be as large as possible in order to minimise the sensitivity values. For the rough surface, however, all three elements are present in the figure of merit. This means that changes in slant angle will have an opposing effect such that the maximum slant angle of 90° is no longer optimal.

VII. Discussion & Conclusions

A *Discussion*

The optimal illumination configuration with regard to tilt angle is considered to be an intuitive result since the three vectors are equally spaced at 120° apart. Previous comment on this issue in the literature only indicated that the planar configuration should be avoided so this is an interesting and potentially useful result.

With regard to optimal slant angle, Woodham's original recommendation [1] is acknowledged. He observed that accuracy in PS would be improved if a large slant angle was used although pointed out that its selection should be balanced against the need to minimise shadowing. He based his argument on the fact that a large slant angle increases the density of the reflectance map. This is desirable because a large change in intensity will result from a small change in the surface gradients, *p* and *q*. In other words Woodham is recommending that the sensitivity of the intensity with respect to the surface gradients is maximised. Our approach to this problem is similar but 'inverted' since we tackle the issue by minimising the sensitivity of the scaled surface normal with respect to the intensity. Indeed, our result for the smooth surface complements that of Woodham's since a slant angle of 90° was found to be optimal. This is obviously the ideal case where shadowing would not be an issue. For a rough surface, we found that the optimal slant angle is 55°. Woodham does not differentiate between types of surfaces except to say that shadowing should be minimised. This would certainly be an issue for a rough surface. We do acknowledge the divergence in results, however, and attribute it to the fact that we minimised the scaled surface normal rather than the surface gradients.

Overall these observations have potential implications for 3-image PS algorithms which select the three 'best' pixel values from multiple images. Once the shadowed and specular intensities have been discarded, it is very possible that the illumination conditions corresponding to the remaining intensities may be less than optimal.

B *Conclusions*

With regard to the placement of the illumination vectors for three-image photometric stereo we found the optimal difference between tilt angles of successive illumination vectors to be 120°. Such a configuration is therefore to be recommended for use with 3-image photometric stereo.

Ignoring shadowing, the optimal slant angle was found to be 90° for smooth surfaces and 55° for rough surfaces. The slant angle selection therefore depends on the surface type.

References

[1] R. J. Woodham, "Photometric method for determining surface orientation from multiple images" Optical Engineering Jan/Feb 1980 Vol. 19 No.1 pp 139 – 144

[2] B. Horn, "Robot Vision", MIT Press, 1986.

[3] J. Blinn, "Simulation of wrinkled surfaces", Computer Graphics (Proc. Siggraph 78), August 1978, pp. 286 – 292.

[4] S. Barsky & M. Petrou, "Colour photometric stereo : simultaneous reconstruction of local gradient and colour of rough textured surfaces", 2001.

[5] G. McGunnigle, "The classification of texture surfaces under varying illumination direction", PhD thesis, Dept. of Computing and Electrical Engineering, Heriot-Watt University, 1998.

[9] H. Rushmeier, G. Taubin, A. Gueziec, "Applying shape from lighting variation to bump map capture", Eurographics Rendering Workshop Proceedings 1997, pp. 35 –44

[10] P. Kube & A. Pentland, "On the imaging of fractal surfaces", IEEE Transactions on Pattern Analysis and Machine Intelligence, 1988, 10(3), pp704-707.

[11] E. N. Coleman, R. Jain, "Obtaining 3-Dimensional Shape of Textured and Specular Surfaces using Four-Source Photometry", Computer Graphics and Image Processing, 18, 309-328, 1982.

[12] K.M. Lee, C.C.J. Kuo, "Shape Reconstruction from Photometric Stereo", Computer Vision and Pattern Recognition '92, Illinois, June 1992.

[13] T. Yamada, H. Saito, S. Ozawa, "3D Reconstruction of Skin Surface from Image Sequence", Proc. Of MVA98: Workshop of Machine Vision Applications, 1998, pp.384-387.

[14] P. Hansson, Per-Ake Johansson, "Topography and reflectance analysis of paper surfaces using a photometric stereo method", Optical Engineering, 39(9), 2555-2561, Sept. 2000.

[15] K. Schlüns, "Shading Based 3D Shape Recovery in the Presence of Shadows", Proc. First Joint Australia & New Zealand Biennial Conference on Digital Image & Vision Computing: Techniques and Applications, Auckland, New Zealand, December 1997, 195-200.

[16] M. J. Chantler, "Why Illuminant Direction is Fundamental to Texture Analysis", IEE Proceedings Vision, Image and Signal Processing, 1995, August Vol.142, No.4, pp.199-206.

[17] A. D. Spence, "Optimal Illumination for Three-Image Photometric Stereo", Research Memo CS2003/02, School of Mathematical & Computing Sciences, Heriot-Watt University, 2003.

• *empirical*
— *theoretical*

- Examples of tertiary tilt angle sweep plots :

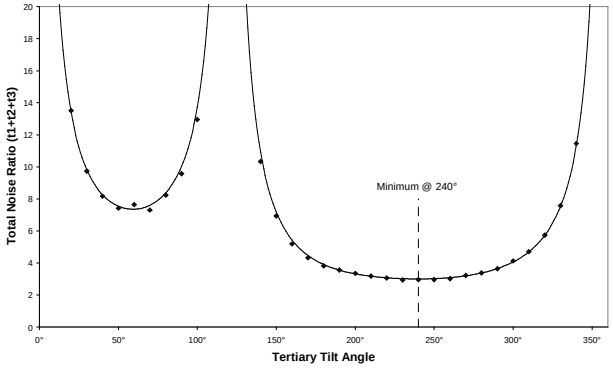

Fig. 3. Noise ratio M_{rough} versus tertiary tilt angle for illumination set [0°,120°,x°].

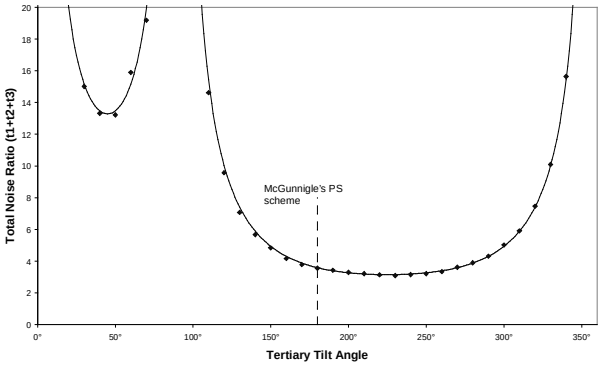

Fig. 4. Noise ratio Mrough versus tertiary tilt angle for illumination set [0°,90°,x°].

- Examples of slant angle ramp plots :

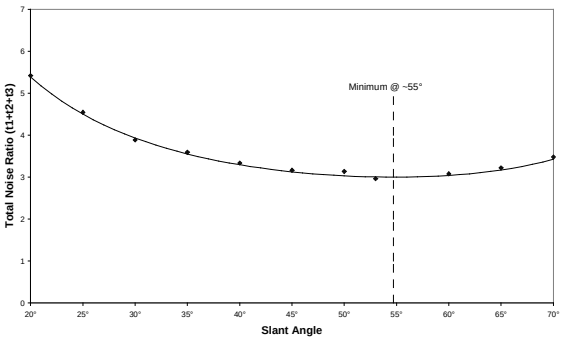

Fig. 5. Total noise ratio Mrough versus slant angle for illumination set [0°,120°,240°].

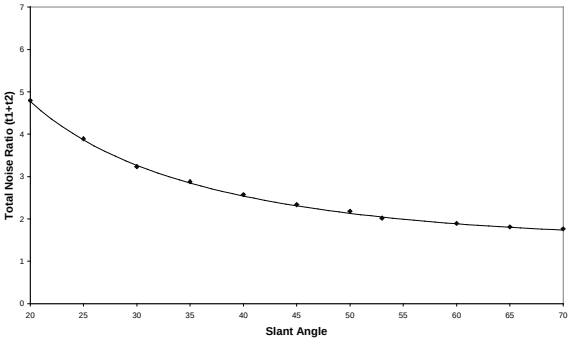

Fig. 6. Total noise ratio Msmooth versus slant angle for illumination set [0°,120°,240°].